



Design, synthesis, and biological evaluation of novel azaspirooxindolinone derivatives as potent inhibitors of ITK and BTK-dependent cancers

Gopal Mudasani^{a,b}, Naveen Kumar Rampeesa^{a,b}, Sreenivasa Reddy Anugu^a, Pullareddy Muddasani^c, Soňa Gurská^{d,e}, Petr Džubák^{d,e}, Marián Hajdúch^{d,e}, Viswanath Das^{d,e,*}, Rambabu Gundla^{b,**}

^a Aragen Lifesciences Pvt. Ltd, Medicinal Chemistry Laboratory Division, Survey No: 125(Part) & 126, IDA Mallapur, Hyderabad 500076, India

^b Department of Chemistry, School of Science, GITAM University, Hyderabad 502102, Telangana, India

^c NATCO Research Center, Sanath Nagar Industrial Area, Sanath Nagar, Hyderabad 500018, Telangana, India

^d Institute of Molecular and Translational Medicine, Czech Advanced Technologies and Research Institute, Palacký University Olomouc, Kržkovského 511/8, 779 00 Olomouc, Czech Republic

^e Institute of Molecular and Translational Medicine, Faculty of Medicine and Dentistry Palacký University and University Hospital Olomouc, Hněvotínská 1333/5, 77900 Olomouc, Czech Republic

ARTICLE INFO

Keywords:

Anti-cancer derivatives
Azaspirooxindolinones
Bruton's tyrosine kinase
Interleukin-2-inducible T-cell kinase
Molecular docking

ABSTRACT

Interleukin-2-inducible T-cell kinase (ITK) and Bruton's tyrosine kinase (BTK) are two important members of the Tec family with crucial roles in immune system function. Deregulation in ITK and BTK activity is linked to several hematological malignancies, making them key targets for cancer immunotherapy. In this study, we synthesized a series of azaspirooxindolinone derivatives and evaluated their cytotoxic activity against ITK/BTK-negative and positive cancer cell lines, followed by enzymatic inhibition studies to assess the ITK/BTK kinase selectivity of two hit compounds. Several compounds demonstrated selective cytotoxicity against ITK- or BTK-expressing cells. Compound **3d** exhibited high cytotoxicity in ITK-positive Jurkat ($IC_{50} = 3.58 \mu M$) and BTK-positive Ramos ($IC_{50} = 3.06 \mu M$) cells, while compound **3j** showed strong cytotoxicity in Ramos ($IC_{50} = 1.38 \mu M$) and Jurkat ($IC_{50} = 4.16 \mu M$) cells. Compounds **3a** and **3e** were selectively cytotoxic in Jurkat cells ($IC_{50} = 9.36 \mu M$ and $10.85 \mu M$, respectively), while compounds **3f** and **3g** were highly cytotoxic in Ramos cells ($IC_{50} = 1.82 \mu M$ and $1.42 \mu M$, respectively). None of the active compounds exhibited cytotoxicity in non-cancer cell lines ($IC_{50} > 50 \mu M$), demonstrating their selectivity for malignant cells. Enzyme inhibition assay showed that **3d** is a selective ITK inhibitor ($IC_{50} = 0.91 \mu M$) with no detectable BTK inhibition, aligning with its strong activity in ITK-positive cells. In contrast, compound **3j** did not inhibit ITK or BTK enzymatically, suggesting an alternative mechanism of action. These findings highlight **3d** as a promising ITK inhibitor and warrant further investigation to elucidate its mechanism of action.

1. Introduction

Interleukin-2-inducible T-cell kinase (ITK) and Bruton's tyrosine kinase (BTK) play pivotal roles in the immune system and have been implicated in human diseases.¹ ITK, primarily expressed in T-cells, regulates T-cell activation and differentiation. Dysregulation of ITK has been associated with various cancers,² highlighting its potential as a therapeutic target in cancer immunotherapy. In contrast, BTK,

predominantly expressed in B cells, is a key component of B-cell receptor signaling. Aberrant BTK activity has been linked to B-cell malignancies, such as B-cell lymphomas and leukemia.³ Targeting BTK, as demonstrated by drugs like ibrutinib, has shown clinical success in treating certain hematologic malignancies.⁴ The roles of ITK and BTK in immune cell signaling underscore their significance in cancer and other human pathogenesis,^{5,6} presenting opportunities for developing targeted therapies against these kinases.

* Corresponding author at: Institute of Molecular and Translational Medicine, Faculty of Medicine and Dentistry Palacký University and University Hospital Olomouc, Hněvotínská 1333/5, 77900 Olomouc, Czech Republic.

** Corresponding author.

E-mail addresses: viswanath.das@upol.cz (V. Das), rgundla@gitam.edu (R. Gundla).

<https://doi.org/10.1016/j.bmc.2025.118116>

Received 4 October 2024; Received in revised form 10 February 2025; Accepted 15 February 2025

Available online 20 February 2025

0968-0896/© 2025 Elsevier Ltd. All rights reserved, including those for text and data mining, AI training, and similar technologies.

Current research in developing inhibitors targeting ITK and BTK holds promise for advancing therapeutic options, especially for immune-related disorders and cancers.⁷ ITK inhibitors are being explored for their potential in modulating T-cell responses and immune-related diseases, focusing on improving specificity and efficacy.^{8,9} Meanwhile, BTK inhibitors continue to be a subject of intense investigation, especially in hematological malignancies.⁷ Amino thiazoles by Bristol-Myers Squibb, amino benzimidazoles by Boehringer Ingelheim, indoles by Sanofi-Aventis, and pyridones by Vertex were among the early compounds designed to target ITK selectively.¹⁰ Ibrutinib, a BTK inhibitor, has already demonstrated clinical success in conditions like chronic lymphocytic leukemia and mantle cell lymphoma.⁷ Although initially designed as a BTK inhibitor, ibrutinib was later found to inhibit ITK due to structural homology.¹¹ Several studies now aim to enhance selectivity and minimize the off-target effects of ITK/BTK inhibitors to develop more effective and safer drug candidates.

In our previous structure–activity relationship (SAR) studies,¹² we found that compound **V** lost anti-proliferative activity compared to similar active compounds (**II**, **III**, **IV**) because the benzodioxyl group at the C-5 position of azaspirooxindoles was replaced with a 3,4,5-trimethoxyphenyl group (Fig. 1). This indicated that the presence of the benzodioxyl group is vital for cytotoxic activity in ITK and BTK-high cell lines. Another common structural feature present in the active compounds causing excellent anti-cancer activity is the α , α -dimethyl functionality (geminal/cyclopropyl) with a heteroatom (fluorine) attached to the carbonyl carbon of the carboxamide functional group (Fig. 1). These results encouraged us to design a new series of compounds based on SAR studies by varying the hydrophilic groups/atoms on α -carbon of the carbonyl group of azaspirooxindoles while retaining the C-5 benzodioxyl group. With these modifications, we designed and synthesized twelve new compounds, two new compounds with C-5 aryl modifications, and one trifluoromethyl sulphonamide derivative. In this study,

we report the synthesis of new azaspirooxindolinone derivatives and their biological activity in a panel of cancer cell lines comprising ITK and BTK-high cancer cell lines.

2. Methods

2.1. Materials

Unless otherwise mentioned, all chemicals were obtained from Lancaster Synthesis (Ward Hill, MA, USA), Sigma-Aldrich (St Louis, MO, USA), and Spectrochem Pvt. Ltd (Mumbai, India), and Combi-Blocks, Inc. (San Diego, CA, USA). All solutions were prepared using deionized distilled water, and all reagents were of analytical grade. The reactions were monitored using thin-layer chromatography (TLC) on an aluminum plate coated with silica gel containing the fluorescent indication F254S. TLC plates were visualized using ultraviolet (UV) light and stained using KMnO_4 and iodine.

^1H NMR and ^{13}C NMR spectra were acquired using an Agilent 400 MHz NMR spectrometer (Agilent Technologies, Inc., Santa Clara, CA, USA). Chemical changes were reported in parts per million (ppm) relative to an internal tetramethylsilane (TMS) standard. The spectral patterns were classified as follows: s (singlet), d (doublet), dd (double doublet), t (triplet), td (triplet of doublet), bs (broad singlet), and m (multiplet). Electrospray ionization (ESI) mass spectra were obtained using a Micromass Quattro LC instrument operating in positive ion mode with a capillary voltage of 3.98 kV. The infrared (IR) spectra were recorded using an FT-IR spectrometer; only significant peaks are in cm^{-1} units.

2.2. Synthesis procedures

Synthesis of 5'-(benzo[d][1,3]dioxol-5-yl)spiro[piperidine-4,3']-

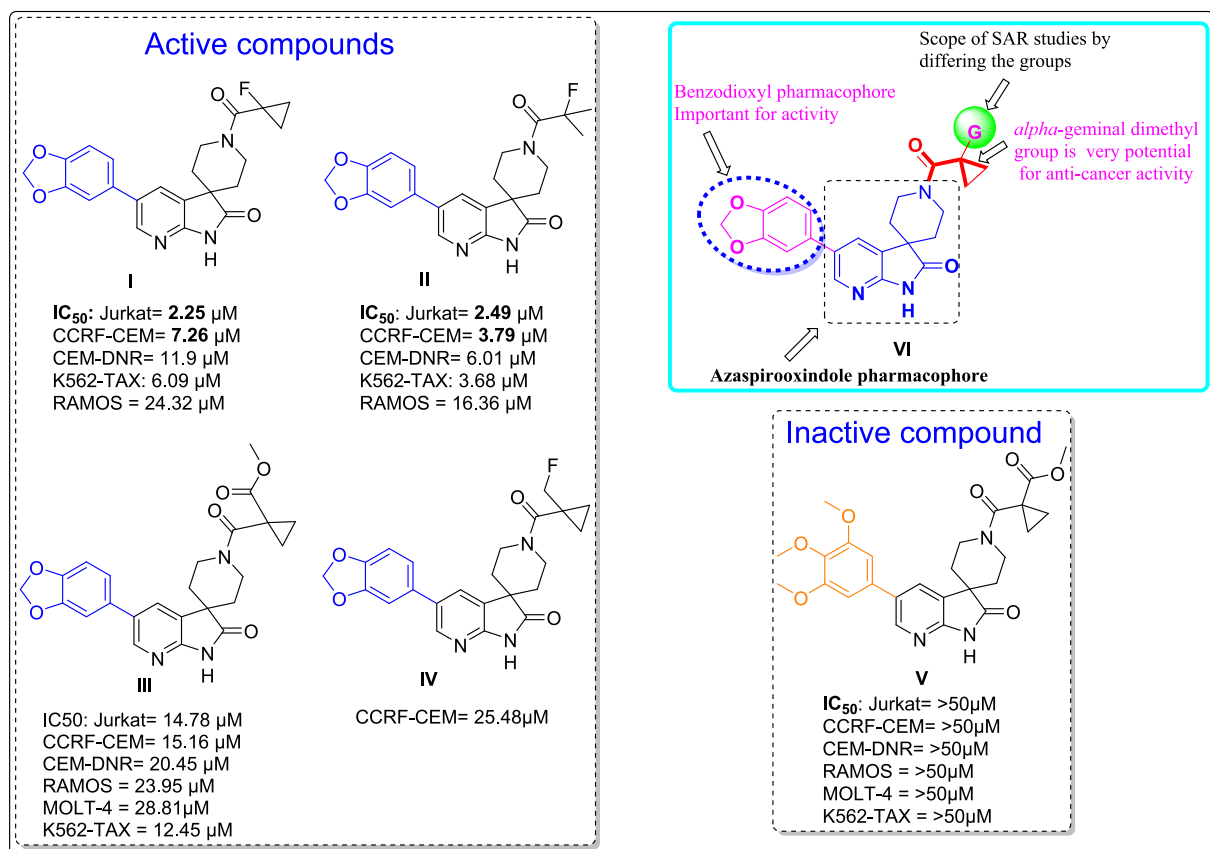


Fig. 1. Design and SAR studies towards new series compounds.

pyrrolo[2,3-*b*]pyridin]-2'(1*H*)-one (1*d*)¹³: Yield: 90 %; Mp: 260–264 °C; White solid.

FT-IR (KBr): ν_{max} 3778, 3605, 3153, 1717, 1611, 1457, 1220, 1038, 810, 688 cm^{-1} . **¹H-NMR (400 MHz, CDCl₃)**: δ 8.27 (d, *J* = 1.6 Hz, 1H), 7.81 (d, *J* = 1.6 Hz, 1H), 6.96–6.99 (m, 2H), 6.89–6.91 (m, 1H), 6.02 (s, 2H), 3.36–3.42 (m, 2H), 3.08–3.14 (m, 2H), 1.96–2.02 (m, 2H), 1.78–1.84 (m, 2H). **¹³C-NMR (100 MHz, DMSO-*d*₆)**: δ 28.32, 43.59, 101.19, 107.17, 108.72, 120.21, 127.23, 129.48, 130.18, 131.59, 144.66, 146.89, 148.02, 155.00, 179.69. **LC-MS ESI**: *m/z* = 324.30 [M + H]⁺.

General procedure for the synthesis of compounds (3a–3i)

To a solution of acid (1.0 equiv.), HATU (1.5 equiv.) and DIPEA (3.0 equiv.) in DMF (0.2 M), the corresponding amine (1.2 equiv.) was added at room temperature. The reaction mixture was stirred at ambient temperature for 2 h, poured onto ice-cold water and stirred for an additional 15 min. The precipitated solid was collected by filtration, washed with water, and dried to obtain the crude compound. Purification was performed using GRACE flash chromatography with a C18, 12 g column, employing 0.1 % formic acid in water and acetonitrile as eluents to yield the final compound.

3-(5'-(Benzo[*d*][1,3]dioxol-5-yl)-2'-oxo-1',2'-dihydrospiro[piperidine-4,3'-pyrrolo[2,3-*b*]pyridin]-1-yl)-2,2-dimethyl-3-oxopropanenitrile (3a): Yield: 40 %; Mp: 258 °C; White solid.

¹H-NMR (400 MHz, DMSO-*d*₆): δ 11.16 (s, 1H), 8.35 (s, 1H), 8.18 (s, 1H), 7.33 (s, 1H), 7.19 (d, *J* = 8.0 Hz, 1H), 6.99 (d, *J* = 8.0 Hz, 1H), 6.05 (s, 2H), 3.98–4.02 (m, 4H), 1.87–1.96 (m, 4H), 1.58 (m, 6H). **¹³C-NMR (125 MHz, DMSO-*d*₆)**: δ 24.98, 24.98, 34.38, 35.47, 35.47, 45.21, 110.09, 107.07, 108.59, 120.08, 122.09, 127.98, 129.64, 129.96, 131.53, 144.15, 146.74, 147.93, 154.92, 165.48, 180.21. **FT-IR (KBr)**: ν (C–O): 1375 cm^{-1} ; ν (C–H bending for methylene): 1454 cm^{-1} ; ν (C=O for amide): 1629, 1724 cm^{-1} ; ν (–NH for amine): 3450 cm^{-1} (–CN peak was not observed). **LC-MS ESI**: *m/z* = 419.2 [M + H]⁺.

5'-(Benzo[*d*][1,3]dioxol-5-yl)-1-(2-hydroxy-2-methylpropanoyl)spiro[piperidine-4,3'-pyrrolo[2,3-*b*]pyridin]-2'(1*H*)-one (3b): Yield: 51 %; Mp: 245 °C; White solid;

¹H-NMR (400 MHz, DMSO-*d*₆): δ 11.15 (s, 1H), 8.34 (d, *J* = 1.2 Hz, 1H), 8.14 (d, *J* = 1.2 Hz, 1H), 7.31 (d, *J* = 0.8 Hz, 1H), 7.18 (d, *J* = 8.0 Hz, 1H), 6.99 (d, *J* = 8.0 Hz, 1H), 6.05 (s, 2H), 4.15–3.80 (m, 4H), 1.96–1.75 (m, 4H), 1.62 (s, 3H), 1.57 (s, 3H). **¹³C-NMR (105 MHz, DMSO-*d*₆)**: δ 12.76, 14.56, 31.20, 45.14, 101.08, 107.02, 108.59, 120.04, 120.18, 127.97, 129.60, 129.96, 131.55, 144.16, 146.74, 147.93, 154.92, 162.61, 180.19. **FT-IR (KBr)**: ν (C–O): 1033 cm^{-1} ; ν (C–N stretching for aromatic amine): 1373 cm^{-1} ; ν (C–O bending for methylene): 1463 cm^{-1} ; ν (C=O for lactum): 1614, 1707 cm^{-1} ; ν (–OH for alcohol): 3552 cm^{-1} . **LC-MS (ESI)**: *m/z* 408.20 [M + H]⁺.

Ethyl 3-(5'-(benzo[*d*][1,3]dioxol-5-yl)-2'-oxo-1',2'-dihydrospiro[piperidine-4,3'-pyrrolo[2,3-*b*]pyridin]-1-yl)-2,2-dimethyl-3-oxopropanoate (3c): Yield: 22 %; Mp: 247 °C; White solid.

¹H-NMR (500 MHz, DMSO-*d*₆): δ 11.15 (s, 1H), 8.33 (d, *J* = 2.4 Hz, 1H), 8.07 (d, *J* = 2.0 Hz, 1H), 7.33 (d, *J* = 1.6 Hz, 1H), 7.17 (dd, *J* = 1.6, 8.0 Hz, 1H), 6.99 (d, *J* = 8.0 Hz, 1H), 6.05 (s, 2H), 4.15 (q, *J* = 6.8 Hz, 2H), 3.93–3.36 (m, 4H), 1.80–1.75 (m, 4H), 1.36 (s, 6H), 1.23 (t, *J* = 6.8 Hz, 3H). **¹³C-NMR (125 MHz, DMSO-*d*₆)**: δ 28.42, 28.42, 40.15, 40.15, 43.47, 55.48, 55.59, 110.47, 112.25, 118.84, 127.33, 129.57, 130.14, 130.41, 144.63, 148.57, 149.16, 154.86, and 179.76; **FT-IR (KBr)**: ν (C–O for ester): 1031 cm^{-10} ; ν (C–O for ester): 1223 cm^{-1} ; ν (C–N stretching for aromatic amine): 1375 cm^{-1} ; ν (C–O bending for methylene): 1462 cm^{-10} ; ν (C=O for lactum): 1649 cm^{-1} ; ν (C=O for ester): 1718 cm^{-1} . **LC-MS (ESI)**: *m/z* = 466.20 [M + H]⁺.

5'-(Benzo[*d*][1,3]dioxol-5-yl)-1-(2,2-difluoropropanoyl)spiro[piperidine-4,3'-pyrrolo[2,3-*b*]pyridin]-2'(1*H*)-one (3d): Yield: 56 %; Mp: 262 °C; White solid.

¹H-NMR (500 MHz, DMSO-*d*₆): δ 8.30 (d, *J* = 1.6 Hz, 1H), 8.07 (s, 1H), 7.62 (d, *J* = 2.0 Hz, 1H), 6.97–6.89 (m, 3H), 6.02 (s, 2H), 4.26–4.14 (m, 3H), 3.90–3.88 (m, 1H), 1.99–1.84 (m, 7H). **¹³C-NMR (125 MHz, DMSO-*d*₆)**: δ 21.96 (t, *J* = 24.8 Hz), 31.18, 31.11, 45.07, 101.07,

107.04, 108.56, 120.03, 127.91, 129.62, 129.95, 131.50, 144.13, 146.73, 147.92, 154.88, 161.28 (t, *J* = 28.8 Hz), 180.17. **LC-MS (ESI)**: *m/z* = 416.2 [M + H]⁺.

5'-(Benzo[*d*][1,3]dioxol-5-yl)-1-(2,2,2-trifluoroacetyl)spiro[piperidine-4,3'-pyrrolo[2,3-*b*]pyridin]-2'(1*H*)-one (3e): Yield: 51 %; Mp: 242 °C; White solid.

¹H-NMR (500 MHz, DMSO-*d*₆): δ 8.30 (d, *J* = 6.0 Hz, 1H), 8.05 (brs, 1H), 7.59 (d, *J* = 2.0 Hz, 1H), 6.97–6.89 (m, 3H), 6.02 (s, 2H), 4.37–4.33 (m, 1H), 4.17–4.15 (m, 1H), 3.94–3.91 (m, 2H), 2.05–1.97 (m, 4H). **¹³C-NMR (125 MHz, DMSO-*d*₆)**: δ 30.94, 31.85, 44.82, 101.11, 106.97, 108.63, 117 (d, *J* = 185.6 Hz), 127.89, 129.55, 129.77, 131.59, 144.20, 146.73, 147.93, 154.17, 155 (d, *J* = 50.8 Hz), 180.53. **FT-IR (KBr)**: ν (C–O): 1215 cm^{-1} ; ν (C–N stretching for aromatic amine): 1375 cm^{-1} ; ν (C–H bending for methylene): 1462 cm^{-1} ; ν (C=O for amide): 1699 cm^{-1} ; ν (–NH for amine): 3458 cm^{-1} . **LC-MS (ESI)**: *m/z* = 420.0 [M + H]⁺.

5'-(Benzo[*d*][1,3]dioxol-5-yl)-1-(1-(trifluoromethyl)cyclopropane-1-carbonyl)spiro[piperidine-4,3'-pyrrolo[2,3-*b*]pyridin]-2'(1*H*)-one (3f): Yield: 62 %; Mp: 245 °C; White solid.

¹H-NMR (500 MHz, DMSO-*d*₆): δ 8.30 (d, *J* = 2.0 Hz, 1H), 7.92 (s, 1H), 7.60 (s, 1H), 6.98–6.9 (m, 3H), 6.02 (s, 2H), 4.18–3.86 (m, 4H), 3.02–1.90 (m, 4H), 1.38–1.36 (m, 2H), 1.23–1.21 (m, 2H). **¹³C-NMR (125 MHz, DMSO-*d*₆)**: δ 9.83, 26.62, 26.88, 31.44, 45.14, 101.13, 107.08, 108.64, 120.10, 124.40, 126.57, 127.99, 129.69, 129.97, 131.61, 144.18, 146.77, 147.96, 154.96, 162.80, 180.25. **FT-IR (KBr)**: ν (C–N stretching for aromatic amine): 1375 cm^{-1} ; ν (C–H bending for methylene): 1462 cm^{-1} ; ν (C=O for lactum): 1647 cm^{-1} ; ν (C=O for amide): 1722 cm^{-1} ; ν (–NH for amine): 3500 cm^{-1} . **LC-MS (ESI)**: *m/z* = 460.20 [M + H]⁺.

1-(5'-(Benzo[*d*][1,3]dioxol-5-yl)-2'-oxo-1',2'-dihydrospiro[piperidine-4,3'-pyrrolo[2,3-*b*]pyridin]-1-carbonyl)cyclopropane-1-carbonitrile (3g): Yield: 59 %; Mp: 267 °C; White solid.

¹H-NMR (400 MHz, CDCl₃): δ 8.30 (d, *J* = 1.6 Hz, 1H), 8.03 (s, residual formic acid from purification, 1H), 7.62 (d, *J* = 2.0 Hz, 1H), 6.98–6.89 (m, 3H), 6.02 (s, 2H), 4.25–4.23 (m, 3H), 3.86–3.84 (m, 1H), 2.06–1.80 (m, 4H), 1.57–1.56 (m, merged in CDCl₃ moisture, 4H). **¹³C-NMR (125 MHz, DMSO-*d*₆)**: δ 28.50, 28.50, 31.87, 31.87, 45.47, 73.14, 101.06, 107.10, 108.58, 120.10, 128.40, 129.52, 129.90, 131.63, 144.06, 146.72, 147.92, 154.93, 173.33, 180.43. **FT-IR (KBr)**: ν (C–N stretching for aromatic amine): 1375 cm^{-1} ; ν (C–H bending for methylene): 1467 cm^{-1} ; ν (C=O for lactum): 1656 cm^{-1} ; ν (C=O for amide): 1712 cm^{-1} ; ν (–NH for amine): 3512 cm^{-1} . **LC-MS (ESI)**: *m/z* = 417.20 [M + H]⁺.

5'-(Benzo[*d*][1,3]dioxol-5-yl)-1-(1-hydroxycyclopropane-1-carbonyl)spiro[piperidine-4,3'-pyrrolo[2,3-*b*]pyridin]-2'(1*H*)-one (3h): Yield: 34 %; Mp: 165 °C; White solid.

¹H-NMR (500 MHz, DMSO-*d*₆): δ 11.13 (s, 1H), 8.33 (d, *J* = 2.0 Hz, 1H), 8.10 (d, *J* = 2.0 Hz, 1H), 7.33 (d, *J* = 1.6 Hz, 1H), 7.18 (dd, *J* = 1.6, 8.0 Hz, 1H), 6.99 (d, *J* = 8.4 Hz, 1H), 6.35 (s, 1H), 6.05 (s, 2H), 4.15–3.78 (m, 4H), 1.82–1.78 (m, 4H), 0.99–0.98 (m, 2H), 0.79–0.78 (m, 2H). **FT-IR (KBr)**: ν (C–H bending for methylene): 1467 cm^{-1} ; ν (C=O for lactum): 1610 cm^{-1} ; ν (C=O for amide): 1720 cm^{-1} ; ν (–OH for alcohol): 3404 cm^{-1} . **LC-MS (ESI)**: *m/z* = 408.20 [M + H]⁺.

1-(5'-(Benzo[*d*][1,3]dioxol-5-yl)-2'-oxo-1',2'-dihydrospiro[piperidine-4,3'-pyrrolo[2,3-*b*]pyridin]-1-carbonyl)cyclopropane-1-carboxylic acid (3i): Yield: 21 % (over two steps); Mp: 267 °C; White solid.

¹H-NMR (500 MHz, DMSO-*d*₆): δ 12.85 (brs, 1H), 11.13 (s, 1H), 8.33 (d, *J* = 2.0 Hz, 1H), 8.04 (d, *J* = 1.6 Hz, 1H), 7.30 (s, 1H), 7.16 (dd, *J* = 1.2, 6.4 Hz, 1H), 6.99 (d, *J* = 6.4 Hz, 1H), 6.05 (s, 2H), 3.93–3.76 (m, 4H), 1.88–1.78 (m, 4H), 1.41–1.21 (m, 4H). **FT-IR (KBr)**: ν (C–N stretching for aromatic amine): 1373 cm^{-1} ; ν (C–H bending for methylene): 1462 cm^{-1} ; ν (C=O for lactum): 1608 cm^{-1} ; ν (C=O for amide): 1718 cm^{-1} ; ν (–COOH): 3458 cm^{-1} . **LC-MS (ESI)**: *m/z* = 436.20 [M + H]⁺.

5'-(Benzo[*d*][1,3]dioxol-5-yl)-1-(2-fluoroacryloyl)spiro

[piperidine-4,3'-pyrrolo[2,3-b]pyridin]-2'(1H)-one (3j): Yield: 47 %; Mp: 269 °C; White solid.

To a solution of compound **1d** (70 mg, 1.0 equiv.), 2-fluoroacrylic acid (2.5 equiv.) and DIPEA (5.0 equiv.) in DMF (2.0 mL), T₃P (50 % in EtOAc, 5.0 equiv.) was added at ambient temperature and the mixture was stirred for 2 h. After completion of the reaction, the mixture was poured into ice-cold water and extracted with ethyl acetate. The combined organic layers were washed successively with water and brine, dried over anhydrous sodium sulfate, and concentrated under reduced pressure to obtain the crude product. The crude product was purified by GRACE flash chromatography using a C18 column with 0.1 % formic acid in water and acetonitrile eluents to afford the title compound as a white solid.

¹H-NMR (500 MHz, DMSO-*d*₆): δ 11.16 (s, 1H), 8.35 (d, *J* = 2.0 Hz, 1H), 8.17 (d, *J* = 2.0 Hz, 1H), 7.33 (d, *J* = 1.6 Hz, 1H), 7.19 (dd, *J* = 1.6, 8.0 Hz, 1H), 6.99 (d, *J* = 8.0 Hz, 1H), 6.05 (s, 2H), 5.33–5.16 (m, 2H), 3.95–3.87 (m, 4H), 1.92–1.84 (m, 4H). ¹³C NMR (125 MHz, DMSO-*d*₆): δ 38.87, 39.07, 39.28, 39.50, 39.71, 39.92, 40.12, 45.25, 98.47, 98.61, 101.16, 107.08, 108.67, 120.09, 128.00, 129.74, 129.99, 131.58, 144.20, 146.80, 148.00, 154.83, 154.97, 157.48, 160.30, 160.61 and 180.28. FT-IR (KBr): ν(C–N stretching for aromatic amine): 1226 cm⁻¹; ν(C–H bending for methylene): 1460 cm⁻¹; ν(C=C for alkene): 1637 cm⁻¹; ν(C=O for lactum): 1660 cm⁻¹; ν(C=O for amide): 1714 cm⁻¹; ν(C–H stretching for alkene): 3113 cm⁻¹; ν(NH): 3446 cm⁻¹. LC-MS (ESI): *m/z* = 396.20 [M + H]⁺.

1-Acryloyl-5'-(benzo[d][1,3]dioxol-5-yl)spiro[piperidine-4,3'-pyrrolo[2,3-b]pyridin]-2'(1H)-one (3k): Yield: 49 %; Mp: 242 °C; White solid.

To a solution of compound **1d** (70 mg, 1.0 equiv.) and DIPEA (10.0 equiv.) in THF (4.0 mL) at 0 °C, acryloyl chloride (1.0 equiv.) was added over 5 min while maintaining the temperature at 0 °C. The resulting reaction mixture was stirred at the same temperature for 5 min. The reaction was quenched upon completion by pouring the mixture into ice-cold water, and the aqueous layer was extracted with ethyl acetate. The combined organic layers were washed successively with water and brine, dried over anhydrous sodium sulfate, and concentrated under pressure to obtain the crude product. The crude compound was purified by GRACE flash chromatography using a C18 column, with 0.1 % formic acid in water and acetonitrile as eluents, to afford the title compound **3k** as a white solid.

¹H-NMR (500 MHz, DMSO-*d*₆): δ 11.12 (s, 1H), 8.34 (d, *J* = 2.0 Hz, 1H), 8.17 (d, *J* = 2.0 Hz, 1H), 7.33 (d, *J* = 1.6 Hz, 1H), 7.19 (dd, *J* = 1.6, 8.0 Hz, 1H), 6.98 (d, *J* = 8.0 Hz, 1H), 6.88 (dd, *J* = 10.4, 17.6 Hz, 1H), 6.15 (dd, *J* = 2.4, 16.8 Hz, 1H), 6.05 (s, 2H), 5.71 (dd, *J* = 2.0, 10.4 Hz, 1H), 3.95–3.87 (m, 4H), 1.90–1.74 (m, 4H). ¹³C NMR (125 MHz, DMSO-*d*₆): δ 31.43, 32.30, 37.05, 40.81, 45.34, 101.14, 107.08, 108.65, 120.06, 127.19, 128.27, 128.52, 129.66, 129.93, 131.59, 144.11, 146.77, 147.98, 154.98, 164.44, and 180.40. FT-IR (KBr): ν(C–N stretching for aromatic amine): 1232 cm⁻¹; ν(C–H bending for methylene): 1462 cm⁻¹; ν(C=C for alkene): 1575 cm⁻¹; ν(C=O for lactum): 1600 cm⁻¹; ν(C=O for amide): 1724 cm⁻¹; ν(C–H stretching for alkene): 3086 cm⁻¹; ν(NH): 3427 cm⁻¹; LC-MS (ESI): *m/z* = 378.62 [M + H]⁺.

5'-(Benzo[d][1,3]dioxol-5-yl)-1-((trifluoromethyl)sulfonyl)spiro[piperidine-4,3'-pyrrolo[2,3-b]pyridin]-2'(1H)-one (3l): Yield: 42 %; Mp: 302 °C; White solid.

To a solution of compound **1d** (60 mg, 1.0 equiv.) and triethylamine (TEA) (5.0 equiv.) in dichloromethane (2.0 mL), triflic anhydride (1.5 equiv.) was added while maintaining the temperature at 0 °C. The resulting reaction mixture was stirred at the same temperature for 2 h. After completion, the reaction mixture was quenched by slowly adding saturated NaHCO₃ solution. The layers were separated, and the aqueous phase was extracted with dichloromethane. The combined organic layers were washed with water and brine, dried over anhydrous sodium sulfate, and concentrated under pressure to obtain the crude product. The crude compound was purified by GRACE flash chromatography

using a C18 column, with 0.1 % formic acid in water and acetonitrile as eluents, to afford the title compound **3l** as an off-white solid.

¹H-NMR (500 MHz, DMSO-*d*₆): δ 11.23 (s, 1H), 8.36 (s, 1H), 8.19 (s, 1H), 7.33 (d, *J* = 1.5 Hz, 1H), 7.20 (dd, *J* = 2.0, 8.0 Hz, 1H), 7.01 (d, *J* = 8.0 Hz, 1H), 6.06 (s, 2H), 3.81–3.84 (m, 4H), 1.91–2.07 (m, 4H). ¹³C NMR (125 MHz, DMSO-*d*₆): δ 31.32, 42.18, 43.97, 101.18, 107.10, 108.70, 120.11, 127.53, 129.78, 130.10, 131.55, 144.39, 146.83, 148.01, 154.95, and 179.95. FT-IR (KBr): ν(S=O for sulfonamide): 1380 cm⁻¹; ν(C–H bending for methylene): 1467 cm⁻¹; ν(C=O for lactum): 1604 cm⁻¹; ν(C=O for amide): 1710 cm⁻¹; ν(NH₂): 3452 cm⁻¹. LC-MS (ESI): *m/z* = 456.0 [M + H]⁺.

1-(2,2-Difluoropropanoyl)-5'-(3,4,5-trimethoxyphenyl)spiro[piperidine-4,3'-pyrrolo[2,3-b]pyridin]-2'(1H)-one (3m): Yield: 41 %; Mp: 210 °C; White solid.

¹H-NMR (500 MHz, DMSO-*d*₆): δ 8.43 (d, *J* = 2.0 Hz, 1H), 8.16 (d, *J* = 2.0 Hz, 1H), 6.91 (s, 2H), 3.87 (s, 6H), 3.80–4.08 (m, 4H), 3.68 (s, 3H), 1.86–1.94 (m, 4H), 1.85 (t, *J* = 20.0 Hz, 3H). FT-IR (KBr): ν(C–O): 1122 cm⁻¹; ν(C–H bending for methylene): 1473 cm⁻¹; ν(C=O for lactum): 1660 cm⁻¹; ν(C=O for amide): 1718 cm⁻¹; ν(NH for amine): 3493 cm⁻¹. LC-MS (ESI): *m/z* = 425.2 [M + H]⁺.

2.3. Computational procedures

2.3.1. Preparation of protein/receptor

The crystal structure of ITK complexed with the inhibitor [4-(carbamoylamino)-1-[7-(propan-2-yloxy)naphthalen-1-yl]-1H-pyrazole-3-carboxamide] and ADP was obtained from the Protein Data Bank (PDB ID-4M15).¹⁴ The downloaded PDB file has a resolution of 2.5 Å. Protein preparation was performed using AutoDock software.¹⁵ The study focused on a single chain that was selected as the investigation subject. The crystal structure lacked its native ligand, non-interacting ions, and water molecules. Efficient hydrogen atoms were incorporated to alleviate the stress on the crystal lattice and render the protein amenable for utilization in the AutoDock docking simulation tool. The protein was generated utilizing the UCSF Chimera graphical user interface after performing structural reduction procedures, including hydrogen atoms, Gasteiger charge calculations, and the consolidation of non-polar hydrogens with carbon atoms.

2.3.2. ChemSketch

ChemSketch was used to draw two-dimensional structures of the synthesized compound, which was then converted into three-dimensional models utilizing its inbuilt algorithms that consider molecular geometry and dynamics. Ligand files were prepared using UCSF Chimera and saved in mol2 file format.¹⁶

2.3.3. Chimera

UCSF Chimera was utilized for molecular visualization and analysis. It offers tools for interactive visualization and analysis of molecular structures, including density maps, docking results, and trajectory analyses.¹⁷

2.3.4. Discovery Studio

Discovery Studio was used to identify interactions between the active sites of the target protein and ligand conformations.¹⁸

2.3.5. Docking

Molecular docking was performed using AutoDock Vina.¹⁵ A grid box for BTK with the dimensions X: 2.866, Y: 8.84, Z: 14.89 Å, and the size of the grid box-22 × 22 × 22, was identified as the protein target docking site and the best molecular interacting compounds were observed. The binding interactions and energies between the ligands and the active site residues were analyzed using Discovery Studio Visualizer.

2.4. Biology

2.4.1. Cell lines

Cell lines were purchased from ATCC (Middlesex, UK) or DSMZ (Braunschweig, Germany) and maintained at 37 °C in a humidified incubator (5 % CO₂/atmospheric air). Cells were cultured in the recommended growth medium supplemented with 10 % fetal calf serum, antibiotics (100 mg/mL streptomycin and 100 U/mL penicillin), 2 mM glutamine, 1 mM sodium bicarbonate, 1 mM sodium pyruvate, and 20 mM HEPES. Cell lines were validated routinely and regularly checked for mycoplasma contamination.

2.4.2. Cytotoxicity assay

The cytotoxicity of the compounds was determined using an MTS assay protocol developed for routine compound screening at our facility. The IC₅₀ values were calculated as described previously.¹⁹ Both chemical and biological data were reported and archived in the MedChemBio Portal (<http://medchembio.imtm.cz>).

2.4.3. Kinase assay

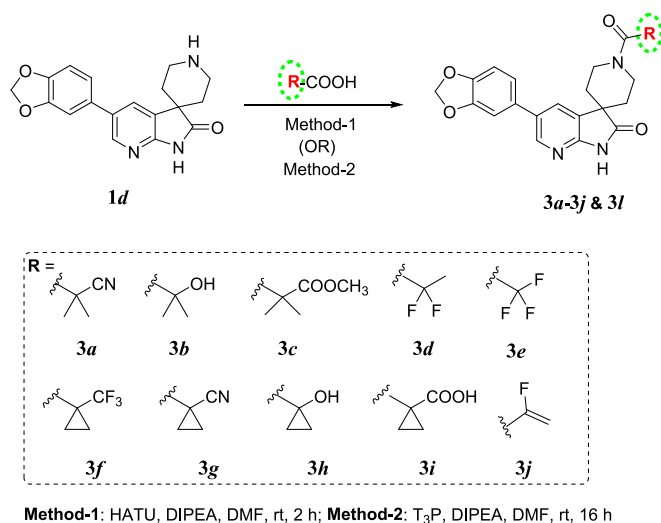
BTK and ITK kinase activity assays were conducted using the BTK Kinase Enzyme System (Cat. #V2941; Promega) and the ITK Kinase Assay Kit (Cat. #78429; BPS Biosciences, Inc.) following the manufacturer's protocol. BTK and ITK enzymes were diluted to 5 ng/μL in 1× kinase reaction buffer. For BTK assays, the buffer was supplemented with 50 μM DTT and 2 mM MnCl₂, as per the manufacturer's instructions. Test compounds (0–10 μM) and ibrutinib (0–100 nM; Cat. #HY-10997; MedChemExpress) were serially diluted in 1× reaction buffer containing 10 % DMSO. These were then dispensed at 1 μL per well in a 384-well white opaque plate (Part #4513; Corning), with a final DMSO concentration of <0.5 % in all reaction wells. The total reaction volume was 5 μL. ADP production was quantified using the ADP-Glo™ Kinase Assay (Cat. #V9101; Promega). Luminescence signals were recorded using a Tecan Infinite 200 PRO plate reader (Tecan Group Ltd., Männedorf, Switzerland) with an integration time of 1000 ms and a settle time of 200 ms. Enzyme activity (%) was determined by normalizing luminescence values against DMSO-treated control wells (100 % activity) and background wells (0 % activity). The half-maximal inhibitory concentration (IC₅₀) values were calculated using a three-parameter logistic model (3PL) in GraphPad Prism (version 10; GraphPad Software, Boston, MA, USA).

3. Results and discussion

3.1. Chemistry

The synthesis of target compounds is outlined in Schemes 1 and 2. Reacting compound 5'-(benzo[d] [1,3] dioxol-5-yl) spiro[piperidine-4,3'-pyrrolo[2,3-b] pyridin]-2'(1'H)-one (**1d**)¹³ with corresponding carboxylic acids using the HATU coupling agent and DIPEA in *N,N*-dimethyl formamide afforded compounds **3a** to **3j** and **3l** in good yields.

The ¹H NMR chemical shift values of geminal dimethyl protons of **3a** are observed at δ 1.58 ppm. In the ¹³C NMR, cyano carbon appeared at δ 201.3 ppm. In ¹H NMR of compound **3b**, the *gem*-dimethyl proton signals were observed at δ 1.50 and 1.62 ppm. In ¹³C NMR, the three carbonyl signals were shifted to a downfield at δ 162.61 and 180.19 ppm. The ethyl signals of ester of compound **3c** were spotted as a triplet at δ 1.23 ppm (*J* = 6.8 Hz) and quartet at δ 4.15 ppm (*J* = 6.8 Hz). In ¹H NMR of compound **3d**, the triplet at δ 1.89 ppm with a high "*J*" value of 20.0 Hz is evidence of methylene protons attached to geminal di-fluorine atoms. In ¹³C NMR of **3d**, the carbon and fluorine two-bond coupling appeared as a doublet at δ 21.92 and 161.28 ppm, with coupling constant values of 24.8 and 28.8 Hz for carbonyl carbon and methyl carbon, respectively. In the ¹³C NMR of **3e**, two bonds of a carbon–fluorine atom of carbonyl carbon appeared as doublet *J*_{C(2)-F} (*J* = 50.8 Hz) at δ 155.0 ppm. The cyclopropyl ring protons of compound **3f** appeared as two sets of



Scheme 1. Synthetic scheme of N-acyl derivatives of azaspirooxindoles.

multiplet between δ 1.21–1.38 ppm. ¹H NMR signals of compound **3h** for cyclopropyl ring proton were seen at δ 0.78–0.99 ppm. The cyclopropyl ring protons of compound **3i** appeared as a multiplet at δ 1.21–1.41 ppm, and two D₂O exchangeable singlets for carboxylic acid and amide protons were spotted at δ 12.58 and 11.13 ppm, respectively.

For the preparation of compound **3j**, the acid–amine coupling between 2-fluoroacrylic acid and corresponding amine (**1d**) was performed under standard conditions using T₃P (50 % solution in ethyl acetate) as coupling reagent and triethylamine base in DMF solvent at ambient temperature for overnight. For compound **3j**, the signals of alkene protons appeared as two doublets of doublets at δ 5.16–5.33 ppm.

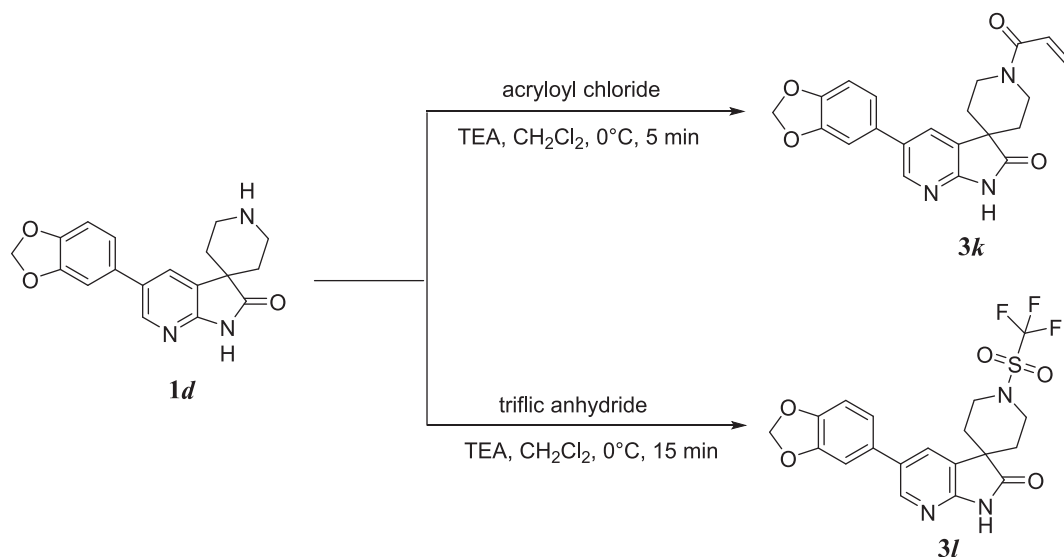
Amidation of **1d** with acryloyl chloride gave the corresponding derivative **3k**. ¹H NMR spectra showed three doublets of doublet signals at δ 6.82, 6.15, and 5.71 ppm with a high coupling constant of 16.8 Hz for *trans* protons of olefin. The reaction of compound **1d** with triflic anhydride presence of triethylamine in dichloromethane resulted in 5'-(benzo[d] [1,3]dioxol-5-yl)-1-((trifluoromethyl)sulfonyl)spiro[piperidine-4,3'-pyrrolo[2,3-b]pyridin]-2'(1'H)-one **3l**. The formation of compound **3l** was confirmed by ¹H NMR, which showed the downfield shift in piperidine ring protons. Besides, the LC-MS spectrum indicated the molecular ion peaks at 456.1 [M + H]⁺.

3.2. Docking-based virtual screening

A docking study was conducted to evaluate the binding affinity and intermolecular interactions of azaspirooxindolinone derivatives with ITK, using ibrutinib as a Ref.²⁰ The crystalline structure of ITK (PDB ID- 4 M15) complexed with compound **9** [4-(carbamoylamino)-1-[7-(propan-2-yloxy) naphthalen-1-yl]-1H-pyrazole-3-carboxamide] and adenosine diphosphate (ADP)¹⁴ was used for Molecular docking.

All 12 azaspirooxindolinone derivatives were docked into the active site of ITK, and their binding energies and molecular interactions were compared with ibrutinib and compound **9** (Table S1). Ibrutinib and compound **9** exhibited a docking score of –9.2 kcal/mol and –9.3 kcal/mol, respectively, interacting with key residues in the ITK active site. Among the compounds, **3d** and **3e** exhibited the same highest docking score of –9.7 kcal/mol. In contrast, **3k** showed the lowest docking energy (–8.7 kcal/mol).

Compound **3d**, later confirmed as an ITK-selective inhibitor, displayed a docking score of –9.0 kcal/mol. It interacted with critical ITK residues, including Gly372, Leu489, Gly441, Met438, Gly370, Val377, Lys391, Ile393, Val507, and Asn487, which have been previously identified as key binding sites for ITK inhibitors.^{21–23} Its binding mode featured conventional hydrogen bonding with Cys442, amide π-stacking



Scheme 2. Synthetic scheme of compound **3k** and **3l**.

with Phe374, and attractive charge interactions with Asp500, suggesting a strong potential for ITK inhibition. 2D ligand interaction diagrams were generated for compound **3d**, highlighting its key interactions within the ITK active site (Fig. 2). Compound **3e** does not form any hydrogen bonds but exhibits significant van der Waals forces and amide π -stacking (Table S1).

Previous pharmacophore-based virtual screening studies have shown that hydrogen bonding with Met438 and Lys391 is essential for ITK inhibition, as these residues contribute to active site stabilization.²¹ The binding interactions of **3d** align well with this model, further supporting its potential as an ITK-selective inhibitor.

Additionally, studies on pyrazolyl-indole derivatives identified Glu436, Met438, and Phe435 as key residues in ITK binding, while Wang et al. found that Phe435, Lys391, Val377, and Ala389 form a distinct hydrophobic pocket that enhances ITK inhibition.^{22,23} Compound **3d** interacted with Val377, Ala389, and Lys391, indicating that it occupies this hydrophobic region, which is known to improve binding affinity.

3.3. *In vitro* anti-cancer activity

The cytotoxic activity of 12 azaspirooxindolinone derivatives and ibrutinib was assessed in a panel of human cancer and non-cancer cell lines representing both male and female origins with varying ITK and BTK statuses (Table 1). The cytotoxicity of these compounds was primarily associated with the ITK/BTK status of the cell lines rather than their sex. Both male- and female-derived ITK/BTK-positive cell lines displayed comparable sensitivity, while ITK/BTK-null lines were generally resistant, indicating that kinase expression plays a more critical role in determining cytotoxic response than cell line sex.

Ramos and K562 cells express several significant B-cell-specific markers, including BTK, whereas Jurkat and CCRF-CEM cells are specific for ITK expression.¹⁹ Most compounds that demonstrated activity in Ramos cells did not exhibit cytotoxic effects in K562 cells. This lack of cytotoxicity in K562 cells is likely attributed to their low levels of BTK expression, possibly due to the presence of the BCR-ABL fusion gene, a recognized primary driver in K562 cells.⁹

Ibrutinib, a positive anti-BTK compound, was highly cytotoxic

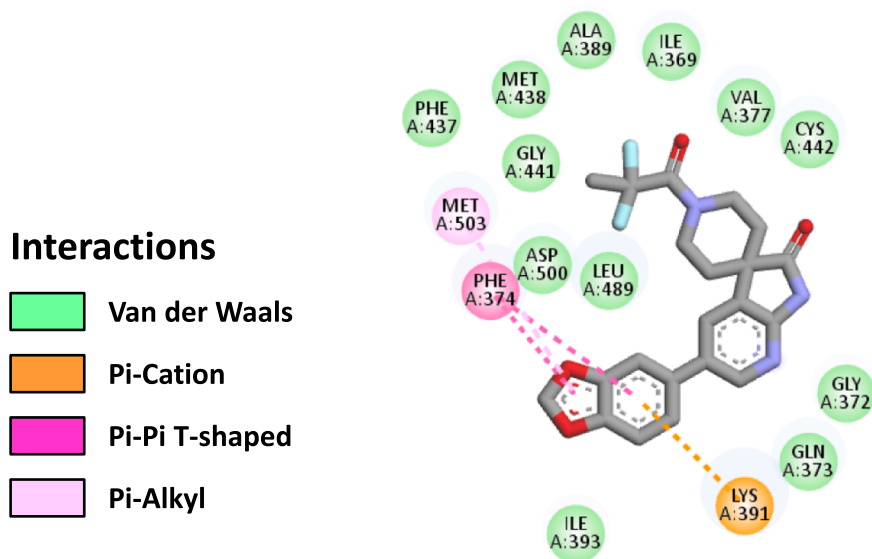


Fig. 2. 2D Ligand interaction diagrams for **3d**.

Table 1

Cytotoxic effects (IC₅₀ values in μM) of azaspirooxindolinone derivatives in a panel of cancer and non-cancer cell lines. Details on cancer type origin, sex, and ITK/BTK status of each cell line are presented in the first column. Data are mean ± SD (n ≥ 6). IC₅₀ values of ibrutinib, previously reported in Ref.,¹⁹ are included for reference.

Cell Line (Cancer type, Sex, ITK/BTK status)	Ibrutinib	3a	3b	3c	3d	3e	3f	3g	3h	3i	3j	3k	3l
A549 (Lung adenocarcinoma, Male, ITK/BTK null)	29.35 ± 3.40	>50	>50	>50	>50	>50	>50	>50	>50	>50	>50	>50	>50
HCT116 (Colorectal carcinoma, Male, ITK/BTK null)	29.82 ± 0.68	>50	>50	>50	>50	>50	>50	>50	>50	>50	>50	>50	>50
U2OS (Osteosarcoma, Female, ITK/ BTK null)	22.61 ± 3.06	>50	>50	>50	>50	>50	>50	>50	>50	>50	18.86 ± 3.34	>50	>50
Jurkat (T-cell leukemia, Male, ITK positive)	5.15 ± 0.70	9.36 ± 0.49	>50	29.24 ± 7.57	3.58 ± 0.36	10.85 ± 1.48	29.41 ± 5.03	50 ± 0	>50	>50	4.16 ± 0.66	>50	>50
CCRF-CEM (T-cell leukemia, Female, ITK positive)	4.25 ± 0.93	14.33 ± 2.06	>50	>50	17.24 ± 3.50	20.72 ± 2.67	19.49 ± 3.74	>50	>50	>50	14.06 ± 2.00	13.45 ± 3.02	>50
Ramos (B-cell lymphoma, Male, BTK positive)	0.29 ± 0.04	10.11 ± 2.13	>50	>50	3.06 ± 0.91	>50	1.82 ± 0.48	1.42 ± 0.13	>50	>50	1.38 ± 0.51	>50	>50
K562 (Myeloid leukemia, Female, BTK positive)	27.36 ± 3.24	>50	>50	>50	>50	>50	>50	>50	>50	>50	>50	>50	>50
MRC-5 (Non-malignant lung fibroblast, Male, ITK/BTK null)	27.86 ± 0.48	>50	>50	>50	>50	>50	>50	>50	>50	>50	>50	>50	>50
BJ (Non-malignant skin fibroblast, Male, ITK/BTK null)	28.91 ± 1.31	>50	>50	>50	>50	>50	>50	>50	>50	>50	>50	>50	>50

against JURKAT, CEM-CCRF, and RAMOS cells, including ITK/BTK null cancer cell and non-malignant fibroblasts (Table 1). However, all synthesized derivatives were inactive against non-cancer cell lines compared to ibrutinib. Compound **1d**, the unmodified core scaffold of our derivatives, was not evaluated in the biological assay, as it exhibited weak activity in our earlier studies against other cancer cell lines.¹³ Based on its limited activity and our SAR principles, we anticipated minimal efficacy for **1d** without functionalization. Thus, we focused on assessing the functionalized derivatives (**3a–3l**) for their potential activity against ITK and BTK.

Compound **3c** (IC₅₀ = 29.24 ± 7.57 μM) showed moderate activity against Jurkat cells, with no activity against Ramos or K562 cells. The cytotoxic activity of **3e** was specific to ITK-positive Jurkat (IC₅₀ = 10.85 ± 1.48 μM) and CCRF-CEM (IC₅₀ = 20.72 ± 2.67 μM) cells, whereas **3g** (IC₅₀ = 1.42 ± 0.13 μM) activity was specific to BTK-high Ramos cells. Other compounds, like **3a**, **3d**, **3f**, and **3j**, showed high-to-moderate activity in Jurkat, CCRF-CEM, and Ramos cells, indicating their possible dual activity against ITK and BTK. Only **3k** (IC₅₀ = 13.45 ± 3.02 μM) showed moderate activity against CCRF-CEM cells. Among the active compounds effective against ITK- or BTK-positive cancer cells, only compound **3j** (IC₅₀ = 18.86 ± 3.34 μM) exhibited moderate cytotoxicity against ITK/BTK-null U2OS cells.

Our SAR investigations began with the synthesis of 5'-(benzo[d][1,3]dioxol-5-yl)-1-(1-fluorocyclopropane-1-carbonyl)spiro[piperidine-4,3'-pyrrolo[2,3-*b*]pyridin]-2'(1'H)-one (**I**).¹² The initial evaluation involved replacing the fluorine atoms with small functional groups. Substitution with —CF₃ and —CN groups yielded compounds **3f** and **3g**, respectively. These compounds exhibited high cytotoxic effects against RAMOS cells, with **3f** (IC₅₀ = 1.82 ± 0.48 μM) and **3g** (IC₅₀ = 1.42 ± 0.13 μM) showing approximately a 20-fold increase in potency compared to compound **I**. However, the introduction of a hydroxyl (—OH) group (**3h**) and carboxylic acid (—COOH) group (**3i**) resulted in decreased activity against RAMOS (IC₅₀ > 50 μM). Notably, the cytotoxic activity of compound **3f** decreased in ITK cell lines, CCRF-CEM (IC₅₀ = 19.49 ± 3.74 μM), and Jurkat (IC₅₀ = 29.41 ± 5.03 μM).

Subsequent SAR investigations focused on *gem*-dimethyl compound 5'-(benzo[d][1,3]dioxol-5-yl)-1-(2-fluoro-2-methylpropanoyl)spiro[piperidine-4,3'-pyrrolo[2,3-*b*]pyridin]-2'(1'H)-one (**II**).¹² Replacing one methyl of the *gem*-dimethyl group with a more electronegative atom, such as fluorine, yielded compound **3d**, which prominently increased potency approximately 5-fold compared to compound **II** against RAMOS cells (**3d**, IC₅₀ = 3.06 ± 0.91 μM). This modification slightly decreased the cytotoxic activity against Jurkat cells (IC₅₀ = 3.58 ± 0.36 μM). Substituting the fluorine atom with the —CN group yielded **3a**, which displayed increased activity ITK and BTK cell lines: RAMOS (IC₅₀ = 10.11 ± 2.13 μM), CCRF-CEM (IC₅₀ = 19.49 ± 3.74) and Jurkat (IC₅₀ = 29.41 ± 5.03 μM).

Interestingly, substituting cyclopropyl or *gem*-dimethyl with an alkene (=CH₂) group resulted in compound **3j**, with an IC₅₀ of 1.38 ± 0.51 μM against RAMOS cells, showing a similar improvement in potency as compounds **3g** and **3f**. These compounds also demonstrated high anti-cancer activity against ITK cell lines, with compound **3j** showing IC₅₀ values of 4.16 ± 0.66 μM against Jurkat and 14.06 ± 2.00 μM against CCRF-CEM cells.

Introducing an α, β-unsaturated methylene (—C=CH₂) group (**3k**) in place of the fluoro cyclopropyl group or fluoro *gem*-dimethyl groups of active compounds **I** and **II** led to moderate anti-proliferative activity against CCRF-CEM cells (IC₅₀ = 13.45 ± 2.00 μM).

The lack of activity (IC₅₀ > 50 μM) observed for compounds **3b** and **3h** indicates that the presence of specific functional groups is crucial for activity. In particular, introducing a hydroxy group instead of the fluorine atoms of compounds **I** and **II**, as in **3b**, may disrupt key interactions within the kinase active site or reduce cell permeability, adversely affecting activity.

3.4. Kinase activity

Due to their cytotoxicity in ITK- and BTK-positive cell lines, **3d** and **3j** were selected to evaluate their effect on ITK and BTK enzyme activity (Fig. 3). Compound **3d** exhibited selective ITK inhibition with an IC₅₀ of

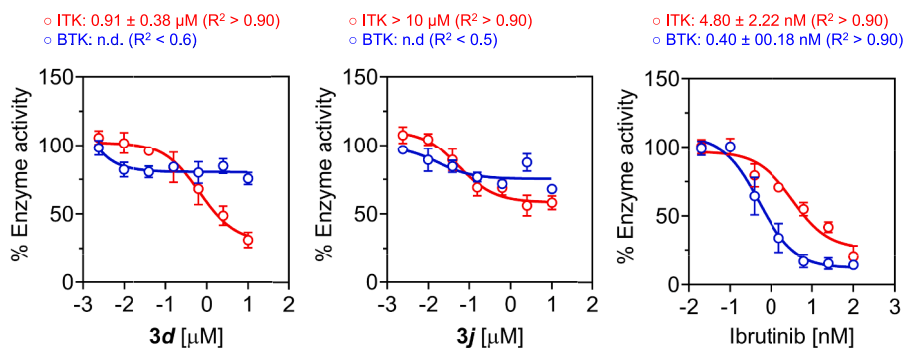


Fig. 3. Dose-response curves showing the effects of **3d** (left), **3j** (middle), and ibrutinib (right) on ITK (red) and BTK (blue) enzyme activity. Curves were fitted using a three-parameter logistic model. Data represent mean \pm SEM ($n = 3$). n.d. – not detectable.

$0.91 \pm 0.38 \mu\text{M}$, while BTK inhibition was not detectable ($R^2 < 0.6$). Compound **3j** showed minimal inhibition of both kinases, with ITK inhibition exceeding $10 \mu\text{M}$ and no detectable BTK inhibition ($R^2 < 0.5$). Ibrutinib exhibited potent inhibition of both ITK and BTK, aligning with its established dual-inhibitory activity. These findings suggest that **3d** acts as a selective ITK inhibitor, whereas **3j** lacks significant ITK or BTK inhibition at enzymatic levels despite its cytotoxic effects in ITK- and BTK-expressing cells.

4. Conclusion

In this study, we synthesized a series of azaspirooxindolinone derivatives and evaluated their cytotoxicity in ITK/BTK-negative and -positive cancer cell lines. From the cytotoxicity screening, compound **3d** demonstrated the highest activity against ITK-positive Jurkat cells and was also potent in BTK-expressing Ramos cells. Compound **3j** showed the strongest cytotoxic effect in Ramos cells and was also active in Jurkat cells. Compounds **3c** and **3g** displayed selective cytotoxicity towards Jurkat and Ramos cells. Importantly, none of the active compounds exhibited cytotoxic effects against non-cancer cell lines. Enzymatic inhibition studies confirmed that **3d** selectively inhibited ITK, with no detectable BTK inhibition, supporting its ITK selectivity. Despite this, **3d**'s cytotoxicity in Ramos cells suggests additional mechanisms beyond direct BTK inhibition, potentially involving off-target kinase interactions or alternative cell death pathways. In contrast, **3j** did not significantly inhibit either ITK or BTK despite its cytotoxic effects in ITK- and BTK-expressing cells, suggesting an alternative mechanism of action. In conclusion, these findings highlight compound **3d** as a promising ITK-selective inhibitor, warranting further investigation into its kinase selectivity, mechanism of cytotoxicity in Ramos cells, and therapeutic potential.

CRediT authorship contribution statement

Gopal Muddasani: Writing – original draft, Methodology, Investigation. **Naveen Kumar Rampeesa:** Methodology, Investigation. **Sreenivasa Reddy Anugu:** Resources, Formal analysis. **Pullareddy Muddasani:** Resources, Formal analysis. **Soňa Gurská:** Methodology, Investigation. **Petr Džubák:** Resources, Funding acquisition. **Marián Hajdúch:** Writing – review & editing, Resources, Funding acquisition. **Viswanath Das:** Writing – review & editing, Supervision, Funding acquisition. **Rambabu Gundla:** Writing – review & editing, Supervision, Funding acquisition, Conceptualization.

Declaration of competing interest

The authors declare the following financial interests/personal relationships which may be considered as potential competing interests: Gopal Muddasani and Naveen Kumar Rampeesa report equipment,

drugs, or supplies were provided by Aragen Life Sciences Private Limited. Gopal Muddasani and Naveen Kumar Rampeesa report equipment, drugs, or supplies were provided by NATCO Research Center, Hyderabad, Telangana. Gopal Muddasani and Naveen Kumar Rampeesa report a relationship with Aragen Life Sciences Private Limited that includes: employment. Gopal Muddasani has patent #Azaspirooxindolinone derivatives and the use of same in cancer therapy (Indian Patent Application No. 202441059533 A) pending to GITAM Deemed to be University. Naveen Kumar Rampeesa has patent #Azaspirooxindolinone derivatives and the use of same in cancer therapy (Indian Patent Application No. 202441059533 A) pending to GITAM Deemed to be University. Sreenivasa Anugu has patent #Azaspirooxindolinone derivatives and the use of same in cancer therapy (Indian Patent Application No. 202441059533 A) pending to GITAM Deemed to be University. Viswanath Das has patent #Azaspirooxindolinone derivatives and the use of same in cancer therapy (Indian Patent Application No. 202441059533 A) pending to GITAM Deemed to be University. Rambabu Gundla has patent #Azaspirooxindolinone derivatives and the use of same in cancer therapy (Indian Patent Application No. 202441059533 A) pending to GITAM Deemed to be University. Both Gopal Muddasani and Naveen Kumar Rampeesa are employees of Aragen Lifesciences Pvt. Ltd, and doctoral students at GITAM deemed to be University. If there are other authors, they declare that they have no known competing financial interests or personal relationships that could have appeared to influence the work reported in this paper.

Acknowledgements

RG acknowledges GITAM University, Hyderabad, India for financial assistance and facility. GR, RN, and RG thank Aragen Lifesciences Pvt Ltd, Hyderabad, India, for providing computational resources for synthesizing and characterizing all the compounds by NMR, LC-MS, and FT-IR. All biological part of the study was supported in parts by the infrastructural projects (CZ-OPENSREEN – LM2023052; EATRIS-CZ – LM2023053), the Czech biobank network (BBMRI - LM2023033), the projects National Institute for Cancer Research (Program EXCELES, ID Project No. LX22NPO5102, Funded by the European Union - Next Generation EU), project SALVAGE (registration number: CZ.02.01.01/00/22_008/0004644, supported by OP JAK, with co-financing from the EU and the State Budget) from the Ministry of Education, Youth and Sports of the Czech Republic (MEYS), and the Project TN02000109 (Personalized Medicine: From Translational Research into Biomedical Applications is co-financed with the state support of the Technology Agency of the Czech Republic as part of the National Centers of Competence Program).

Appendix A. Supplementary material

Supplementary data to this article can be found online at <https://doi.org/10.1016/j.bmc.2025.118116>.

Data availability

All data supporting the findings of this study are available in the manuscript or [Supplementary files](#). Cytotoxicity data of compounds are stored in the IMTM Dotmatics database and MedChemBio Portal and available from the corresponding author (V. Das) upon reasonable request.

References

- Shoji K, Suzuki A, Okamoto M, et al. Prolonged shedding of infectious viruses with haplotype switches of SARS-CoV-2 in an immunocompromised patient. *J Infect Chemother*. 2022;28:1001–1104. <https://doi.org/10.1016/j.jiac.2022.04.004>.
- Lechner KS, Neurath MF, Weigmann B. Role of the IL-2 inducible tyrosine kinase ITK and its inhibitors in disease pathogenesis. *J Mol Med (Berlin)*. 2020;98:1385–1395. <https://doi.org/10.1007/s00109-020-01958-z>.
- Garg N, Padron EJ, Rammohan KW, Goodman CF. Bruton's tyrosine kinase inhibitors: the next Frontier of B-cell-targeted therapies for cancer, autoimmune disorders, and multiple sclerosis. *J Clin Med*. 2022;11, 6139. <https://doi.org/10.3390/jcm11206139>.
- Davids MS, Brown JR. Ibrutinib: a first in class covalent inhibitor of Bruton's tyrosine kinase. *Future Oncol*. 2014;10:957–967. <https://doi.org/10.2217/fon.14.51>.
- Nadeem A, Ahmad SF, Al-Harbi NO, et al. Inhibition of Bruton's tyrosine kinase and IL-2 inducible T-cell kinase suppresses both neutrophilic and eosinophilic airway inflammation in a cockroach allergen extract-induced mixed granulocytic mouse model of asthma using preventative and therapeutic strategy. *Pharmacol Res*. 2019; 148, 104441. <https://doi.org/10.1016/j.phrs.2019.104441>.
- Molina-Cerrillo J, Alonso-Gordoa T, Gajate P, Grande E. Bruton's tyrosine kinase (BTK) as a promising target in solid tumors. *Cancer Treat Rev*. 2017;58:41–50. <https://doi.org/10.1016/j.ctrv.2017.06.001>.
- Ran F, Liu Y, Xu Z, et al. Recent development of BTK-based dual inhibitors in the treatment of cancers. *Eur J Med Chem*. 2022;233, 114232. <https://doi.org/10.1016/j.ejmech.2022.114232>.
- Zhou D, Zuo Y, Pan Z. Discovery of potent and highly selective interleukin-2-inducible T-cell kinase degraders with in vivo activity. *J Med Chem*. 2023;66: 4979–4998. <https://doi.org/10.1021/acs.jmedchem.2c02078>.
- Wang X, Xue G, Pan Z. Design, synthesis and structure-activity relationship of indolylindazoles as potent and selective covalent inhibitors of interleukin-2 inducible T-cell kinase (ITK). *Eur J Med Chem*. 2020;187, 111918. <https://doi.org/10.1016/j.ejmech.2019.111918>.
- Norman P. Inducible tyrosine kinase inhibitors: a review of the patent literature (2010–2013). *Expert Opin Ther Pat*. 2014;24:979–991. <https://doi.org/10.1517/13543776.2014.936381>.
- Dubovsky JA, Beckwith KA, Natarajan G, et al. Ibrutinib is an irreversible molecular inhibitor of ITK driving a Th1-selective pressure in T lymphocytes. *Blood*. 2013;122: 2539–2549. <https://doi.org/10.1182/blood-2013-06-507947>.
- Mudasani G, Paidikondala K, Gurská S, et al. C-5 Aryl substituted azaspirooxindolinones derivatives: synthesis and biological evaluation as potential inhibitors of tec family kinases. *Eur J Org Chem*. 2021:4630–4640. <https://doi.org/10.1002/ejoc.202100699>.
- Mudasani G, Paidikondala K, Gundla R, Maddirala SJ, Das V. Synthesis and biological evaluation of 5'-arylspiro[piperidine-4,3'-pyrrolo-[2,3-b]pyridin] analogues. *ChemistrySelect*. 2021;6:3378–3381. <https://doi.org/10.1002/slct.202004719>.
- Han S, Czerwinski RM, Caspers NL, et al. *Biochem J*. 2014;460:211–222. <https://doi.org/10.1042/BJ20131139>.
- Morris GM, Huey R, Lindstrom W, et al. AutoDock4 and AutoDockTools4: automated docking with selective receptor flexibility. *J Comp Chem*. 2009;30: 2785–2791. <https://doi.org/10.1002/jcc.21256>.
- Hunter AD. ACD/ChemSketch 1.0 (freeware); ACD/ChemSketch 2.0 and its Tautomers, Dictionary, and 3D Plug-ins; ACD/HNMR 2.0; ACD/CNMR 2.0. *J Chem Edu*. 1997;74:905.
- Pettersen EF, Goddard TD, Huang CC, et al. UCSF Chimera—a visualization system for exploratory research and analysis. *J Comput Chem*. 2004;25:1605–1612. <https://doi.org/10.1002/jcc.20084>.
- Discovery studio. D Studio. Accelrys [2.1] 420; 2008.
- Koraboina CP, Maddipati VC, Annadurai N, et al. Synthesis and biological evaluation of oxindole sulfonamide derivatives as Bruton's tyrosine kinase inhibitors. *ChemMedChem*. 2024;19, e202300511. <https://doi.org/10.1002/cmde.202300511>.
- Marcotte DJ, Liu YT, Arduini RM, et al. Structures of human Bruton's tyrosine kinase in active and inactive conformations suggest a mechanism of activation for TEC family kinases. *Protein Sci*. 2010;19:429–439. <https://doi.org/10.1002/pro.321>.
- Bagga V, Silakari O, Ghorela VS, Bahia MS, Rambabu R, Sarma J. A three-dimensional pharmacophore modelling of ITK inhibitors and virtual screening for novel inhibitors. *SAR QSAR Environ Res*. 2011;22:171–190. <https://doi.org/10.1080/1062936X.2010.510480>.
- Velankar AD, Quintini G, Prabhu A, et al. Synthesis and biological evaluation of novel (4 or 5-aryl)pyrazolyl-indoles as inhibitors of interleukin-2 inducible T-cell kinase (ITK). *Bioorg Med Chem*. 2010;18:4547–4559. <https://doi.org/10.1016/j.bmc.2010.04.056>. Epub 2010 Apr 24.
- Pastwa E, Somiari RI, Malinowski M, Somiari SB, Winters TA. In vitro non-homologous DNA end joining assays—the 20th anniversary. *Int J Biochem Cell Biol*. 2009;41:1254–1260. <https://doi.org/10.1016/j.biocel.2008.11.007>.